scientific reports



OPEN

Land productivity declines in the GGW while human contributions to restoration far outweighing degradation

Yubo Zhi^{1,2,3}, Xiaosong Li^{1,2⊠}, Tong Shen^{1,2}, Graciela Metternicht⁴, Anne Grainger⁵, Yude Pan^{6⊠}, Qi Lu⁷ & Amos Tiereyangn Kabo-Bah⁸

The African Great Green Wall (GGW) initiative is a major effort to achieve the Sustainable Developed Goals (SDG) 15.3 target of Land Degradation Neutrality (LDN) in the Sahel regions. This study provides a comprehensive assessment of the land productivity dynamics (LPD) within the GGW from 2013 to 2022, serving as a sub-indicator for SDG 15.3.1 reporting and analyzes the key factors influencing these changes. Our results indicate that the land degradation outpaces restoration in the GGW, with 4.93% of the area experiencing declining land productivity (LP) compared to only 3.44% showing improvement. This suggesting that the effectiveness of the GGW initiative has not met expectations, highlighting the need for more targeted interventions. Among the drivers of LPD, we found that land cover change (LCC) accounts for the largest share of LPD increase (30.97%), while climate change (CLI) is the main contributor to declining LP (43.51%). The impact of CO₃ fertilization is similar to that of LCC, whereas nitrogen deposition (NDE) has a minimal influence. Among human-driven factors, forest loss, cropland abandonment and deforestation for cultivation are the primary causes of declining LP. Conversely, forest expansion and reclamation of bare land for agriculture are the main contributors to increasing LP. Our findings demonstrate that while climate change remains a major challenge, human-driven land management strategies can play a pivotal role in restoring degraded land. The GGW initiative requires more coordinated, science-based strategies to achieve its full potential by 2030. By integrating climate adaptation, land restoration policies, and sustainable land-use practices, the GGW can enhance both ecological resilience and community livelihoods across the Sahel.

The Sahel region, one of the most vulnerable areas to land degradation due to desertification^{1–3} climate change^{4,5} and unsustainable land use practices^{6,7} faces compounded challenges from population pressure⁸ widespread poverty⁹ and land use conflicts. It plays a critical role in global efforts to achieve Land Degradation Neutrality (LDN), which aims to combat desertification, restore degraded land and soil, under the United Nations Sustainable Development Goals (SDG 15.3)^{10,11}. Launched in 2007, the African Great Green Wall (GGW) initiative aims to combat desertification and land degradation across the Sahel region by restoring 100 million hectares of degraded land by 2030^{2,7}. As such, it is a cornerstone of global LDN efforts.

While some progress has been made——such as restoring 4 million hectares of land and planting millions of trees in countries like Senegal and Ethiopia¹². The initiative has also attracted significant international attention and funding, with \$14 billion pledged in 2021 to support its implementation. By 2023, numerous editorials have focused on the progress of the GGW, which noted that, as of 2020, the GGW had achieved only 4–20% of its 2030 targets^{2,13,14} with this figure varying depending on the reporting standards applied. These discrepancies highlight the lack of standardized metrics for evaluating the initiative's true progress.

Consequently, employing more precise monitoring methods and higher-resolution data is critical to accurately assess the current rate of land degradation and evaluate how restoration progress counters this degradation. A potential solution is to adopt the United Nations' LDN progress assessment indicators¹⁵ as achieving LDN is one

¹Aerospace Information Research Institute, Chinses Academy of Sciences, Beijing, China. ²International Research Center of Big Data for Sustainable Development Goals, Beijing, China. ³University of Chinese Academy of Sciences, Beijing, China. ⁴School of Science, Western Sydney University, Richmond, Australia. ⁵School of Geography, University of Leeds, Leeds, UK. ⁶USDA Forest Service, Durham, NH, USA. ⁷Institute of Ecological Conservation and Restoration, Chinese Academy of Forestry, Beijing, China. ⁸Department of Civil and Environmental Engineering, University of Energy and Natural Resources, Sunyani, Ghana. [⊠]email: lixs@aircas.ac.cn; yude.pan@usda.gov

of the primary and core objectives of the GGW, which ensure alignment with the SDG framework and provide better guidance for structured evaluation. This is particularly crucial as 2023 marks the mid-term evaluation of LDN progress¹⁶. Therefore, conducting a spatially and temporally explicit assessment (2015–2022) of the GGW is of great importance. LDN monitoring relies on three core sub-indicators: land cover, land productivity and soil organic carbon (SOC)¹⁵. While SOC is a critical component of land degradation assessments, it remains underresearched in the Sahel due to significant data gaps, particularly at regional scales. Remote sensing data, including MODIS^{3,17} and Landsat¹⁸ imagery, have been extensively used to analyze land cover changes⁶ providing valuable insights into spatial and temporal trends. Land productivity, typically measured using satellite-based indices such as the Normalized Difference Vegetation Index (NDVI)¹⁹ and Enhanced Vegetation Index (EVI)²⁰ is the most variable indicator and is highly influenced by climate variability^{21,22} making it a key point of contention in the Sahel region.

Our motivation stems from the current lack of clarity in assessing the progress of the GGW, necessitating a reliable evaluation framework, and the need to elucidate the impacts of key drivers—particularly climate and human activities—on land productivity changes. In this study, we analyzed land productivity changes in the GGW from 2015 to 2022 and their driving factors to assess the progress of both the LDN target and the GGW initiative. First, we generated a high-resolution (30-meter) land productivity dynamic (LPD) dataset to capture finer-scale land productivity changes in arid and semi-arid regions²³ surpassing the commonly used 250-meter²⁴ or 1-kilometer^{25,26} resolution datasets. Second, we applied the Lindeman–Merenda–Gold (LMG)²⁷ method to quantify the relative importance (RI) of factors such as precipitation, radiation, temperature, rising CO₂, nitrogen deposition (NDE), forestland fractional changes (FFC) and cropland fractional changes (CFC) in shaping LPD trends. Finally, we examined the role of human activities in different LPD classes to provide insights into the effectiveness of land management practices in the GGW region.

Results

LPD results and Spatial difference

The 30-meter LPD map for the GGW area from 2013 to 2022, generated using the HiLPD-GEE tool²³ is shown in Fig. 1 (also see Supplementary Fig. 1). The LPD effectively reflects the trajectory of land productivity (LP) over a given period and categorizes it into five levels: declining, early signs of decline, stable but stressed (Negative fluctuation), stable and not stressed (Positive fluctuation), and increasing LP²⁸. The results indicate that the "stable but not stressed" class accounts for the largest proportion (40.26%), primarily concentrated in the northern GGW region (Fig. 1 and Supplementary Table 1). The "declining" and "early signs of decline" classes represent 4.93% and 17.8% of the total area, respectively, with most of these lands located in the southern region of Nigeria's GGW. Meanwhile, the "increasing" class (3.44%) is predominantly observed in Nigeria, Sudan, and Mali.

At the national level, Nigeria has the largest area of declining LP $(5.99\times10^4~{\rm km^2}$ but also the largest area of increasing LP $(3.31\times10^4~{\rm km^2})$. The difference between increasing and declining classes (D_{I-D}) at the country level shows that Burkina Faso has the most negative D_{I-D} (-9.73%), while Eritrea has the highest positive value D_{I-D} (11.34%) (Supplementary Table 1). These results highlight substantial areas where land degradation outpaced restoration efforts, underscoring the challenges and urgent tasks associated with achieving the GGW's restoration objectives.

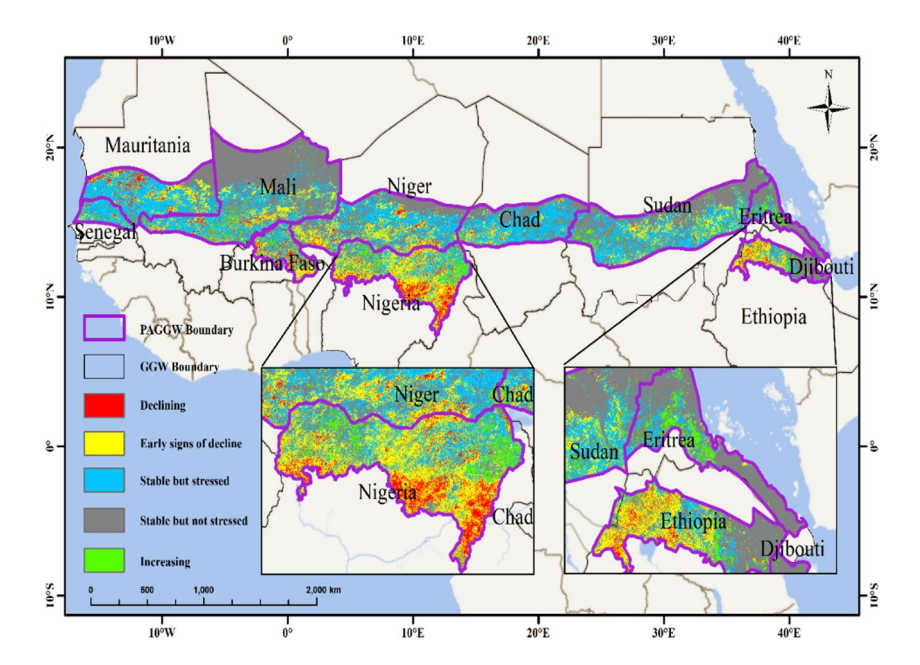


Fig. 1. 30 m LPD spatial distribution map. The area where EVI < 0.1 is filled with the stable and not stressed type.

We also compared the LPD results with those of the Mann-Kendall trend analysis using NDVI, a method commonly employed in previous studies ^{18,19,29,30} with results shown in Fig. 2. Although NDVI indicates greening significantly outweighs browning (Supplementary Fig. 2), LPD reveals a more nuanced picture. Based on LPD classification criteria, areas were categorized as "agree" (NDVI trends align with LPD) or "disagree" (NDVI trends differ from LPD). Most regions fall into the "agree" category, but discrepancies are notable in greening areas, where 86% of NDVI-classified "greening" pixels are categorized as "Stable but not stressed" under LPD. These pixels, often in sparsely vegetated areas (EVI < 0.1), show increased vegetation cover but lack stable or significant LP improvement. Similarly, 24% of NDVI-classified "browning" areas are also "Stable but not stressed" in LPD, primarily in low-vegetation regions, as these areas are excluded from LPD calculations.

Driver factors for LPD

We used Lindeman–Merenda–Gold (LMG) method (see Methods)²⁷ to assess the relative influence of various factors on LPD, by decomposing the R² statistic into proportional contributions for each driver (Supplementary Fig. 3). This method provides a robust estimate of each driver's unique contribution to LPD variations.Our analysis shows that LPD is affected variously by precipitation (15.46%), temperature (13.70%), radiation (14.66%), nitrogen deposition (NDE) (11.70%), rising CO₂ (21.48%, the dominant factor), forestland fractional changes (FFC) (11.14%), and cropland fractional changes (CFC) (11.88%).To better interpret these driving factors, we grouped the factors to four categories, Climate Change (CLI), Land Cover Change (LCC), NDE and rising CO₂. Our results show that LPD is most affected by CLI, followed by LCC and rising CO₂, although spatial variability is high (Fig. 3a). At the national level (Fig. 3b and Supplementary Table 2), central Sahel countries such as Mali, Niger, Chad, and Burkina Faso are strongly influenced by rising CO₂, while coastal nations like Mauritania, Senegal, and Sudan are more affected by CLI. Notably, in Djibouti and Eritrea, LCC plays most significant role in determining LPD.

By analyzing the relationship between each factor and latitude (Supplementary Fig. 4), we found that as latitude increases, the influence of rising CO₂, precipitation, and temperature on LPD also intensifies, increasing by 1.32%, 0.43%, and 0.38% per 1° increase in latitude, respectively. In contrast, the influence of radiation and NDE gradually weakens, decreasing by 0.33% and 0.14% per 1° increase in latitude, respectively. Particularly, in arid environments (Fig. 4a), the impact of rising CO₂ on LPD strengthens significantly, underscoring its role of a key driver of productivity change in these areas. Additionally, in regions where cropland and forestland coexist, cropland's relative importance (RI) increases with latitude (by 0.65% per degree), while forestland's RI decreases (by 0.18% per degree) (Fig. 4b). This suggests that in higher latitudes croplands contribute more to LPD, whereas forests contribute relatively less. The transition point between the two factors is located at approximately 13.5°N. In the northern region, which is predominantly arid and hyper-arid, bare land is the dominant land cover type (Supplementary Fig. 5), agricultural activities have a stronger impact on LPD. In contrast, the more humid southern regions exhibit a stronger influence of forestland on LPD. The 13.5°N line marks both the boundary between arid and semi-arid areas and the divide between dominant agricultural and forestry activities. We refer to this transition zone as the "Boundary" in subsequent discussions.

Further analysis of cropland and forestland coverage in the GGW region reveals substantial changes (Supplementary Fig. 6), with significant forestland fractional changes (FFC) covering approximately 4×10^5 km² and significant cropland fraction changes (CFC) covering 2.5×10^5 km². About 60% of forestland has undergone significant degradation, while approximately 83% of cropland has expanded (Fig. 4e). Moreover, the extent of cropland expansion outpaces that of forest degradation (Fig. 4e).

By analyzing land cover changes across the "Boundary", we observe that in the southern region, forestland degradation accounts for 71.9% of total land cover changes, with 66.06% of these area simultaneously experiencing cropland expansion (Fig. 4d). Additionally, 23.37% of the region shows simultaneous forest and cropland expansion, primarily in southern Sudan and areas around Djibouti. In the northern region, concurrent cropland and forestland expansion is widespread (51.41%), particularly in the eastern Sahel (Fig. 4c). However, the rate (slope) of cropland expansion in the north significantly surpasses forest cover change (Fig. 4e). Meanwhile, 20.79% of the northern region experiences simultaneous degradation of both cropland and forestland, particularly in the western Sahel (Fig. 4c). In summary, the southern regions of the "Boundary" appear to be experiencing extensive

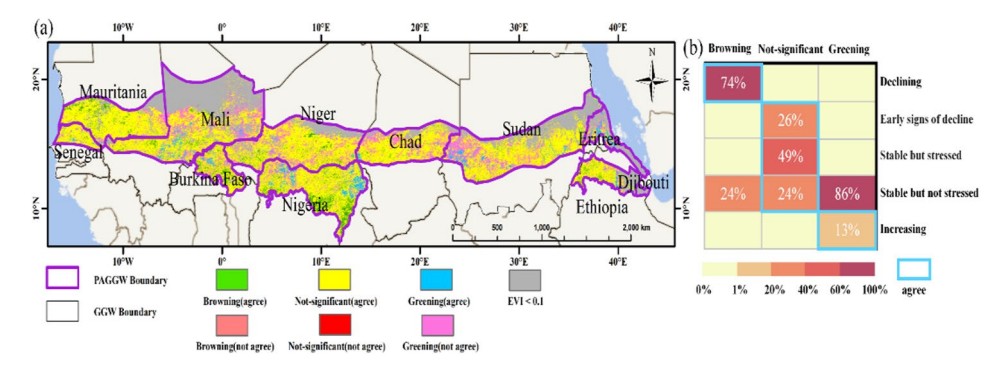


Fig. 2. Comparison of LPD and M-K results and confusion matrix. **(a)** Comparison of LPD and M-K results. **(b)** Confusion matrix.

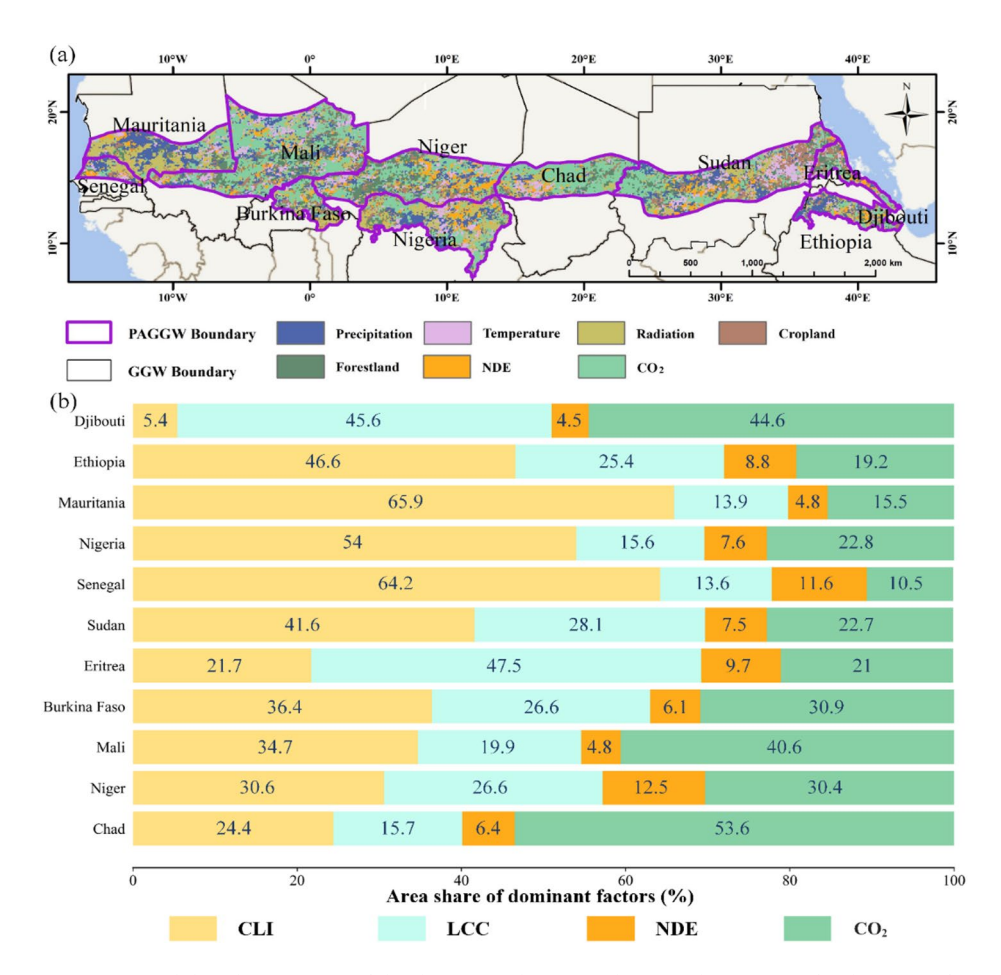


Fig. 3. Spatial distribution map of the dominant drivers and national statistics. The dominant factor defined as the driving factor that has the largest RI. (a) Spatial distribution map of the dominant drivers. (b) National statistics. Climate change (CLI) that is comprised of temperature, precipitation, and radiation; land cover change (LCC) of FFC and CFC.

deforestation driven by agricultural expansion, though further analysis is needed to confirm this hypothesis. In contrast, cropland expansion is the dominant trend north of the "Boundary", while changes in forest coverage are relatively limited.

Difference of driver factors for different LPD classes

By comparing the different LPD classes (Supplementary Table 3), we found that areas classified as "early signs of declining" experience the most pronounced impact from CLI (49.93%). The influence of NDE remains relatively constant across classes at approximately 11%. Rising $\rm CO_2$ emerges as the dominant factor across all LPD classes, with its impact peaking in the "increasing" class (29.15%), except in the "early signs of decline" class.

Notably, areas with declining LP are more strongly influenced by CLI (43.51%) than areas with increasing LP (29.6%). Conversely, LCC has greater impact on areas with increasing LP (30.97%) than on decline (22.73%) (Fig. 5). This suggests that LCC is the strongest driver of land productivity increase, surpassing CLI in positive trends, while CLI remains the dominant driver of LPD decline —— almost doubling the effect of LCC. FFC contributes significantly to increasing LP, second only to rising $\rm CO_2$, with a 1.42 times stronger impact on increasing LP (17.48%) compared to declining LP (12.29%). Additionally, using Cliff's Delta, we quantified the magnitude of RI differences between increasing and declining LPD classes, where larger absolute values signify greater differences. Results show that RI of all factors, except NDE, exhibits significant differences between the two LPD levels. These findings underscore the crucial role of LCC, particularly FFC, in enhancing land productivity. Meanwhile, $\rm CO_2$ fertilization effects are widespread and strong, whereas NDE has the least impact on LPD changes.

Main LCC types in different LPD classes

To further investigate LPD, we analyzed cropland and forestland cover within areas of significant increasing and declining LP. Results show that cropland expansion occurs in both across increasing and declining LPD classes (Fig. 6a). However, no significant difference was found between RI and cropland coverage changes across these two classes (Fig. 6b). In contrast, forestland coverage follows a distinct pattern. As LPD transitions from decreasing to increasing classes, changes in forestland coverage shift from negative to positive values (Fig. 6c).

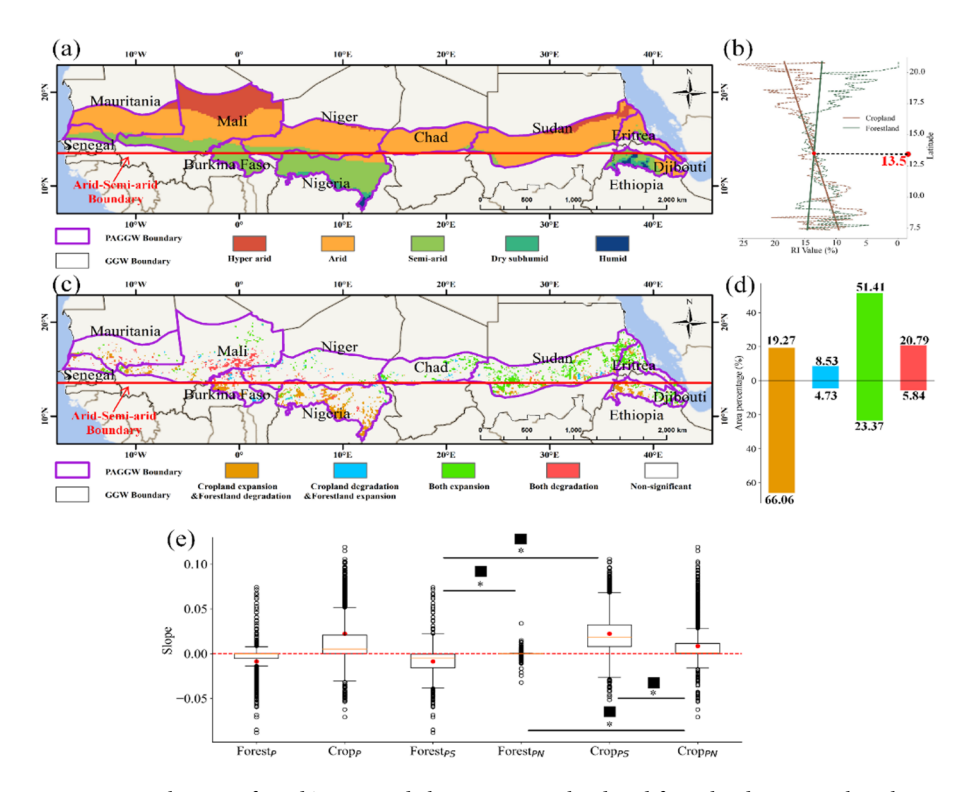


Fig. 4. Distribution of Arid Zones and changes in cropland and forestland cover within the GGW Region. (a) Map of aridity. The bioclimatic zone is defined by the Aridity Index (AI) following the classification developed by FAO. The red solid line represents "Boundary". (b) The variation of RI of CFC and FFC with latitude. We only considered areas where forestland or cropland existed. The dashed line represents the mean RI along the latitude direction, while the intersection points of the fitted lines (solid lines) for forestland and cropland RI are marked by red dots. (c) Map of significant changes in forestland and cropland cover, detailed in Supplementary Fig. 6. Utilizing sen's slope estimator and the Mann-Kendall (M-K) trend test, we obtained the trends of cropland and forestland fractional changes between 2015 and 2022. (d) The percentage of change type north and south of the "Boundary". (e) Statistics of categories and slope conditions on both sides of the "Boundary". The subscript "P" denotes significant results from the M-K test, while the subscripts "N" and "S" represent areas north and south of "Boundary", respectively. *P<0.001. In addition, Cliff's Delta can be used to calculate the effect size of the Mann-Whitney U test. The larger the effect size, the greater the difference. ■: Large effect size.

Notably, all forestland in declining LPD class exhibits degradation, whereas the vast majority of forestland in increasing LPD class shows expansion (Fig. 6d). This suggests a strong correlation between the direction of forestland change and LPD classes: forestland expansion is linked to LPD increases, while forestland degradation corresponds to LPD decreases. Furthermore, larger forestland changes correspond to higher RI (Fig. 6d), reinforcing the idea that forest expansion plays a critical role in improving land productivity.

We also analyzed the inflow and outflow patterns of forestland and cropland types within significant LPD areas. Results show that forest degradation is primarily driven by transitions to shrubland and cropland, with 90.92% and 96.28% of these areas, respectively, showing LP declines (Supplementary Table 4). Cropland, on the other hand, is mainly converted to bareland and shrubland, with 73.5% and 52.6% of these areas experiencing LP declines, respectively. Meanwhile, forest expansion primarily originates from shrubland, with 85.79% of the expanded areas showing LP increases (Supplementary Table 5). Cropland expansion occurs mainly through the conversion of bare land, shrubland, and forest. While 77.26% of bare land conversions lead to LP increases, 82.08% of shrubland conversions and 96.28% of forest conversions result in LP declines. These results indicate that LP declines are primarily associated with forest loss, cropland abandonment, and deforestation due to cultivation, whereas forest expansion and bare land reclamation are mainly linked to LPD increases.

Discussion

Land productivity change status

Previous studies have extensively examined vegetation greening at global ^{19,20,29,30} Sahelian ^{5,6,17,31–35} and national scales ^{36,37} primarily focusing on the period from 1982 to 2015. Most research has suggested a general greening trend in the Sahel since 2000 ^{14,16,17,27,28}. However, some studies indicate that the Leaf Area Index (LAI) in the Sahel has started to decline since 2000 ³¹, while in the Guinean Savannahs region of Nigeria (NGS), land degradation (38%) has significantly outpaced restoration (14%) from 2003 to 2018 ³⁶.

Our study reveals that during 2013–2022, LP in the GGW region exhibited an overall decline, with degraded areas covering 4.93% of the total land area, while restored areas accounted for 3.44%. This finding contrasts

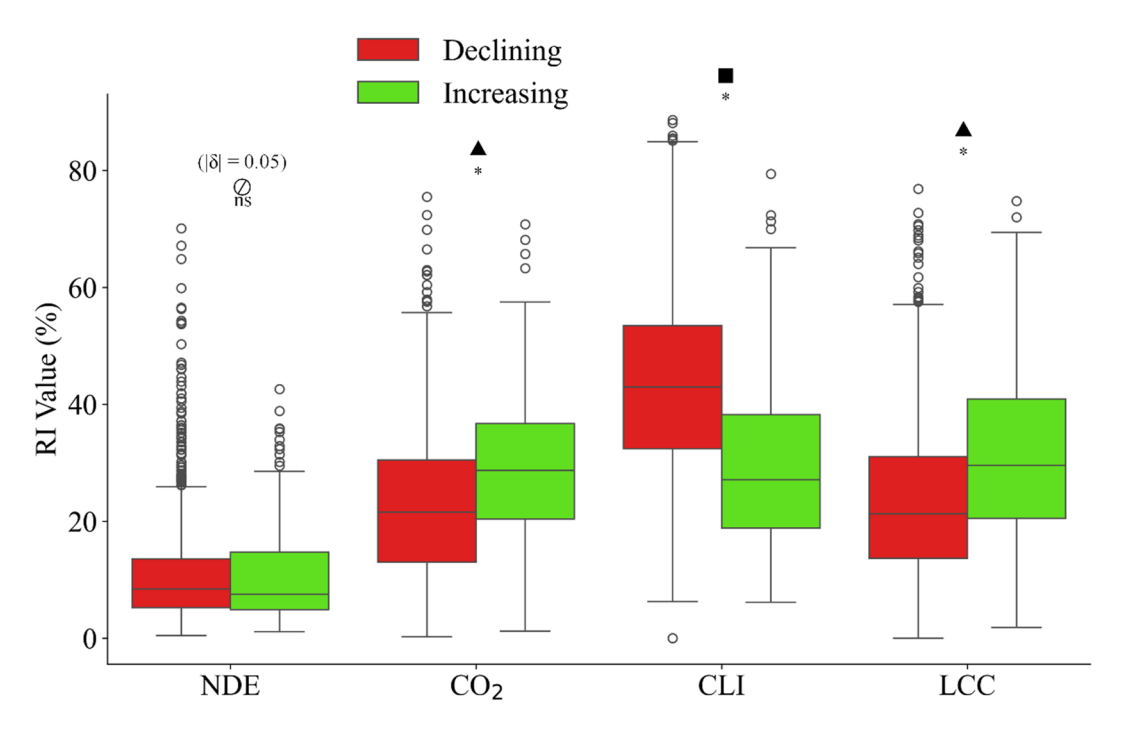


Fig. 5. Differential drivers analysis between increasing and declining Classes. CLI (Precipitation, Temperature, Radiation), LCC (FFC, CFC) represent cumulative factors within their respective categories. Given the evident skewness in the distribution, we utilized the Mann-Whitney U test to detect significant differences. *P<0.001; ns denotes non-significance. Cliff's Delta is used to calculate the effect size for the Mann-Whitney U test. ⊘: Non-significant effect size. ▲: Medium effect size. ■: Large effect size.

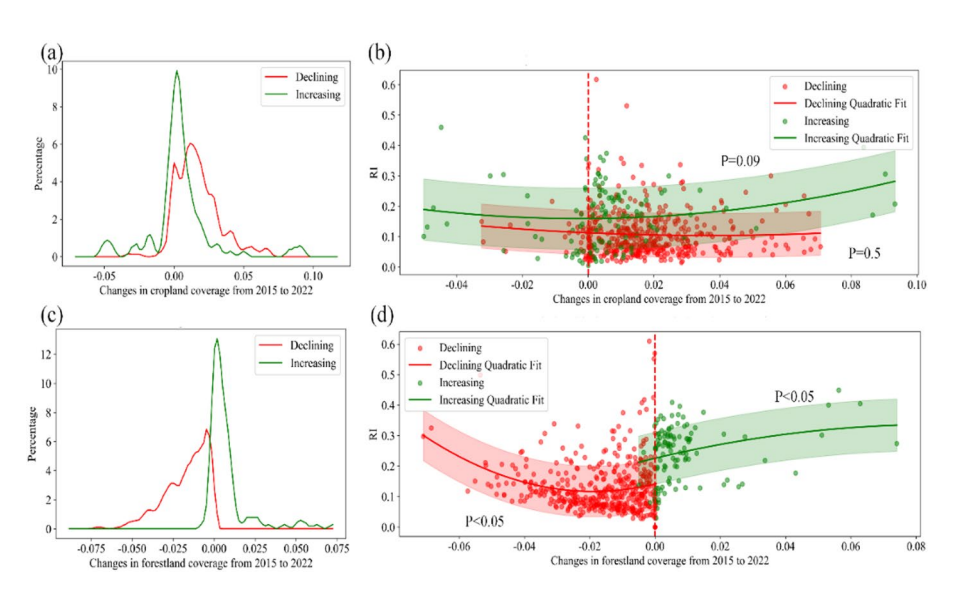


Fig. 6. Relationship between land cover change (LCC) and relative importance (RI). Among them, **(a-b)** are about cropland, **(c-d)** are about forestland. **(a)** and **(c)** Distribution of changes in cropland and forestland coverage in increasing and decreasing class from 2015 to 2022. **(b)** and **(d)** are the relationship between slope and RI in two cases, and are fitted with quadratic functions. "P < 0.05" means the fitting equation is significant.

with the previous studies that reported widespread greening trends (Fig. 2 and Supplementary Fig. 2). The discrepancy arises due to differences in the calculation methods. Our approach integrates multiple indicators to provide a more comprehensive evaluation for regional land productivity characteristics. Unlike traditional NDVI trend analyses, our LPD methodology incorporates three additional indicators^{23,25,28}: Multi-Temporal Image Difference (MTID)oxy_comment_end²⁵ Initial Biomass, and Stage Change. This integration allows a more detailed assessment of stable and chaging productivity conditions. 86% of the pixels classified as "greening" fall under as the LPD category "Stable but not stressed", indicating that while vegetation cover may

have increased, it has not necessarily translated into significant improvement in land productivity. These pixels either do not meet the required stability and magnitude for productivity changes^{23,25,28} or are located in sparsely vegetated areas (Supplementary Fig. 5), making it difficult to confirm a stable increase in land productivity. These results demonstrate that the LPD method, by integrating more comprehensive indicators, offers more accurate identification of land productivity (i.e. stable increases or decreases), providing a more holistic evaluation of vegetation dynamics and land-use efficiency^{23,25}.

Spatial heterogeneity of driver RI

Land productivity in the Sahel is influenced by a combination of factors³⁹including climate change^{4,32}increased human activities⁶ and rising CO₂²⁰. Using the LMG method, we quantified the RI of these drivers. Our results indicate that rising CO₂ is the dominant factor across the GGW region (Fig. 3b), with an average RI of 21.48% (Supplementary Table 2), consistent with the findings of Jian et al.²⁹. The rising CO₂ significantly enhances vegetation greenness in semi-arid areas by alleviating plants' dependency on water³⁹. Our results indicate that precipitation (RI = 15.46%) emerges as the second most influential factor (Supplementary Table 2), consistent with prior studies suggesting that rainfall is a key driver of greenness changes in the Sahel^{18,19}. Given that much of the region consists of semi-arid and arid landscapes (Fig. 4a), vegetation remains highly sensitive to precipitation variability⁴⁰⁻⁴². Additionally, rainfall in the Sahel has been steadily increasing since 2000^{31,43-45}, further influencing LPD trends. NDE has a relatively smaller impact across the region (RI = 11.7%), in agreement with earlier studies^{18,46} indicating that nitrogen is not a limiting factor in tropical forests, grasslands, savannas, or shrublands. While net primary productivity (NPP) is sensitive to nitrogen addition and increased precipitation⁴⁶nitrogen availability is generally sufficient in the Sahel, reducing its influence on LPD.

Land cover change (LCC), represented by cropland fractional changes (CFC) and forestland fractional changes (FFC), has a lower average impact on land productivity than climate change (CLI) (Supplementary Table 2). Its impact on LP is subject to human intervention^{7,36,37}. The average RI across the GGW region may not fully capture their role in areas with significant productivity changes, highlighting the importance of distinguishing between overall RI patterns and localized effects. Therefore, it is crucial to accurately distinguish the roles of climate change and human activities in land productivity changes. Notably, we found that LCC accounts for the highest share of LP increases (30.97%) – even surpassing climate change factors (Supplementary Table 3). This finding aligns with Wu et al.³³ and Burrell et al.⁴⁷who identified LCC as a major driver of vegetation greenness changes. Compared to degraded areas, CFC and FFC play a larger role in increasing LP (Supplementary Table 3), highlighting the effectiveness of human interventions like afforestation and land reclamation. Despite slow progress in the GGW² and ongoing degradation in some areas, these findings underscore the potential of sustainable land management to enhance productivity while supporting economic and ecological restoration⁷.

Characteristics of human activities in areas with increasing and declining LP

Deforestation is a dominant land-use trend in tropical regions³⁹. Our study reveals widespread deforestation and cropland expansion south of the "Boundary" (Fig. 4e). Meanwhile, cropland expansion is particularly pronounced north of the "Boundary", where bareland is the dominant land cover type, especially in Sudan (Fig. 3e and Supplementary Fig. 5). Overall, forest loss and cropland expansion are the predominant land cover changes, with cropland expansion outpacing the decrease of forestland (Fig. 4e). This pattern is consistent with previous studies on land-use change in Sub-Saharan Africa^{48,49} and GGW-participating countries^{36,50-52}.

However, the impact of cropland expansion on LPD is complex: it contributes modestly to LP increases but also drives declines in some areas (Fig. 6b). In contrast, forestland changes show a much clearer relationship with LPD: deforestation leads to widespread LP decline while forestland expansion contributes significantly to LP increases, with the impact strengthening as the magnitude of forestland change grows (Fig. 6d). Forest loss, farmland abandonment, and deforestation for cultivation have been the primary drivers of LP decline (Supplementary Tables 4 and 5), and FFC exerts a stronger influence than CFC in these areas as well (Supplementary Table 3). Studies in Sub-Saharan Africa⁴⁸ West Africa⁴⁹ and GGW participating countries^{7,36,50} all indicate that wood extraction for fuel and subsistence agriculture is the primary cause of deforestation, which may lead to significant land degradation³⁶. Shifting agriculture has been a common driver of forest disturbances in sub-Saharan Africa from 2001 to 2015⁵⁴. Approximately 38% of the Guinean Savannahs region of Nigeria (NGS) has experienced land degradation, primarily due to unsustainable agricultural practices³⁶while 14% of the land in the NGS has shown improvement due to reforestation efforts and drought-resistant species planting by local governments³⁶. Since 2000, most African countries have experienced significant agricultural growth, strongly contributed to GDP increases^{54,55}. However, nearly 75% of this growth is attributed to increased cultivated areas rather than yield improvement⁵⁵. This expansion model, However, comes at the expense of ecological sustainability, further complicating progress toward achieving SDG 15.3.

Despite the predominance of forest loss and degradation in the GGW region, our findings demonstrate that forest expansion plays a crucial role in LP restoration, while cropland expansion has a more region-specific impact on productivity trends. This underscores the importance of integrating land restoration measures such as afforestation and bareland reclamation into broad land management policies^{7,36,37}. Future strategies should holistically address agricultural expansion, forest protection, and restoration to ensure sustainable land productivity and support the GGW initiative.

Methods Study area

This study focuses on the GGW region, which aim to address land degradation, desertification, climate change impacts across Sahel. The initiative involves 11 countries, including Ethiopia, Chad, Niger, Mali, and others. The Sahel is recognized as a "hotspot" for achieving SDG 15.3.1 due to its vulnerability to land degradation. The

annual average temperature in the GGW region exceedes 25 °C, with an altitude range of -330 to 4529 m. Annual rainfall varies significantly, ranging from 0 to 1000 mm and gradually increasing from north to south²³. Near the southern Sahel border, there is 450-500 mm of annual rainfall, while less than 200 mm at higher latitudes⁴. The GGW is a semi-arid transition zone between the tropical rainforest in southern Africa and the arid northern desert³⁴. During periods of severe drought, vegetation in the Sahel has undergone extensive degradation and loss, though some recovery has occurred with increased rainfall⁵⁶. The GGW boundary used in this study was provided by The Pan African Agency of the Great Green Wall (PAGGW).

Data and preprocessing

We selected 7 key driving factors for analysis, including temperature, radiation, precipitation, forestland fraction changes (FFC), cropland fraction changes (CFC), rising CO_2 and NDE. Given the large disparities in spatial resolution among datasets, we standardized the resolution and coordinate system before analysis. Specifically, for datasets with resolutions greater than 10,000 m, we applied bilinear interpolation using resample() and reproject() functions in Google Earth Engine (GEE) to downscale them to a uniform 10,000 m resolution in the WGS84 coordinate system. For datasets with resolutions below 10,000 m, we used ee.reduceRegion() with ee.Reducer.mean() to aggregate values. To accurately assess spatiotemporal patterns of vegetation greenness dynamics from 2015 to 2022, we used a high-quality fused NDVI dataset²³ applying gapfilling and GF-SG filtering techniques.

We extracted temperature, precipitation, and radiation data from the ERA5-Land Daily Aggregated dataset (GEE Collection Snippet: ECMWF/ERA5_LAND/DAILY_AGGR), selecting the temperature_2m, total_precipitation_sum, and surface_solar_radiation_downwards_sum bands. To assess the driving effect of changes in land use types on LPD, we used Google's DYNAMIC WORLD V1 dataset⁵⁷ which provides detailed land cover changes at a 10-meter resolution. This dataset categorizes land into eight types: water, trees, grass, flooded vegetation, crops, shrub & scrub, built areas, bareland, and snow & ice (Supplementary Fig. 5). In this study, the distribution dynamics of crops and trees types are used to explore LPD. Since this dataset produces land cover data on a daily basis, ee.Reducer.mode() is applied on the time-filtered collection to select the most frequently occurring class label for each pixel during the year. We calculated and mapped annual cropland and forestland coverage (2015 to 2022), at a 10,000-meter resolution. We further generated 30-meter resolution land cover maps by calculating the mode of each pixel within a 3×3 neighborhood to matchwith the 30-meter LPD data.

Rising CO₂ Data was obtained from Zenodo based on the SSP-126 scenrios (downloaded from https://zenodo.org/records/5021361⁵⁸). We used the monthly average to calculate the annual mean CO₂ concentration (2015–2022). Nitrogen deposition (NDE) data was sourced from the NASA Goddard Institute for Space Studies (GISS) as part of the Atmospheric Chemistry and Climate Model Intercomparison Project (ACCMIP) (downloaded from https://data.ceda.ac.uk/badc/accmip/data/GISS/GISS-E2-R/accrcp60/ACCMIP-monthly/r1i1p3/v1). We used annual total deposition values from dry and wet deposition datasets, calculated from monthly depositions. The Aridity Index (AI) data was derived from the Global Aridity dataset released by CGIAR Consortium for Spatial Information (CGIAR-CSI), calculated as the reciprocal of the aridity index values. The AI is defined by the United Nations Environmental Programme (UNEP)⁵⁹. The drought zone classification is based on FAOdefined thresholds(https://data.apps.fao.org/catalog/dataset/221072ae-2090-48a1-be6f-5a88f061431a/reso urce/7563c7fa-03aa-4141-92ef-8aa4236fb9a4). Vegetation indices were from the MODIS EVI dataset (GEE Collection Snippet: MODIS/061/MOD13Q1)⁶⁰, which was used for long-term vegetation monitoring.

LPD calculation

To effectively assess LPD at high spatial resolution, we employed HiLPD-GEE tool²³ to produce 30 m and 10,000 m LPD datasets (2013 to 2022). The LPD methodology incorporates three additional NDVI-derived indicators^{23,25,28}: Multi-Temporal Image Difference (MTID)²⁵Initial Biomass, and Stage Change, which refine the assessment of land productivity dynamics. LPD was classified into five classes: declining, early signs of decline, stable but stressed, stable and not stressed, and increasing land productivity. HiLPD-GEE can realize 30 m LPD calculation in any spatial range and time window around the world after 2013²³. After that, to minimize false detections by NDVI, we applied an EVI>0.1 mask to exclude sparsely vegetated areas from classification. These areas were reassigned to "stable and not stressed".

Driving factor RI calculation

Before calculating the RI, all factor data (2015–2022) were z-score normalized across the entire GGW region. That is, the eight-year data are standardized using the mean and variance of the eight-year factor data. We hypothesize that LPD result from a combination of climate change, human activities, and atmospheric influences. To evaluate the contribution of each driver, we applied the Lindeman–Merenda–Gold²⁷ (LMG) method, which quantifies the impact of predictors independent of order effects, estimates the RI of these factors to NDVI, and ultimately obtain the spatial pattern of each driving factor in the region. We constructed the multiple linear regression equation of precipitation, temperature, radiation, CFC, FFC, NDE and rising CO_2 for NDVI annual changes in each grid. Therefore, NDVI can be expressed in the following form:

$$NDVI = a_0 + \sum_{i=1}^{7} a_i x_i + \varepsilon \tag{1}$$

where x_i represents precipitation, radiation, temperature, precipitation, FFC, CFC, NDE and rising CO_2 . ϵ represents other possible drivers of NDVI changes. In multiple regression models, the RI assessment depends heavily on the order of the regressors. The metric LMG can be written as

$$LMG(x_k) = \frac{1}{p!} \sum_{S \subseteq \{x_1, \dots, x_p\} \setminus \{x_k\}} n(S)! (p - n(S) - 1)! seqR^2(\{x_k\} | S).$$
(2)

where $n\left(S\right)$ refers to the number of elements in the set S. This formula shows LMG (x_k) as the average over average contributions in models of different sizes²⁷. The R^2 for a model with regressors in set S is given as

$$R^{2}(S) = \frac{\text{Model SS (model with regressors in S)}}{\text{Total SS}}.$$
(3)

The additional R^2 when adding the regressors in set $\{x_k\}$ to a model with the regressors in set S is given as

$$seqR^{2}(\{x_{k}\}|S) = R^{2}(\{x_{k}\}\cup S) - R^{2}(S).$$
 (4)

The LMG method estimates the RI of each variable by decomposing the sum of squares into the non-negative contribution shared by each variable, and the LMG values were computed by averaging the sequential sum of squares (R^2 across all factor orderings. Final RI values were normalized (divided by R^2 to sum to 1^{19} . We implemented the variance decomposition algorithm based on the multiple linear regression model on the GEE platform. In each grid cell, we calculated the contribution of each factor to the interannual NDVI. During the calculation process, the forestland proportion and cropland proportion in some areas may be zero, causing the calculation results in these areas to be masked. To address missing values, RI calculations were performed separately for areas: with only forestland, with only cropland, with both land types, and without either. We calculate the RI where the factor value exists respectively. For example, in an area where only forestland exists, we calculate the RI of precipitation, temperature, radiation, FFC, CFC, NDE and rising CO_2 , and filter it with a mask where forestland exists but cropland does not exist. Finally, each category was aggregated to obtain spatial RI distribution patterns for each factor.

Statistical analysis

To discern the distributional disparities of factors' RI under scenarios of increasing and decreasing land productivity, we used the 10,000 m LPD data and the Mann-Whitneyu (M-W) test from the scipy.stats package in Python. This test assesses whether samples adhere to probability distributions with identical medians. Cliff's Delta was then used to assess the degree of difference. Cliff's Delta^{61,62}also known as δ , is a measure of effect size used to quantify the difference between two groups or conditions in non-parametric statistics. It provides a standardized measure of the magnitude of the difference between two distributions, such as groups of scores or rankings, which may not meet the assumptions required for parametric tests like t-tests or ANOVA. It can avoid misinterpretation of statistically significant but minor effects due to the large sample sizes⁶³. Cliff's Delta ranges from -1 to 1, where 0 indicates no difference between the two groups. Values closer to 1 or -1 indicate larger differences, with the sign indicating the direction of the difference. Cliff's Delta (δ) is calculated using the following formula⁶²:

$$\delta = \frac{\text{Number of observations where } y_i > x_j - \text{Number of observations where } y_i < x_j}{n_y \times n_x}$$
 (5)

 y_i represents an observation from group y, x_j represents an observation from group x, n_y is the number of observations in group y, n_x is the number of observations in group x. In this study, our criteria for judging effect sizes are as follows: non-significant effect, $|\delta| < 0.11$; small effect: $0.11 \le |\delta| < 0.28$; medium effect: $0.28 \le |\delta| < 0.43$; large effect: $|\delta| \ge 0.43^{64}$.

After evaluating the driving effects of cropland fractional changes and forestland fractional changes on LPD, we aim to clarify the actual changes in cropland and forestland. We used the M-K trend test and Sen's slope analysis to detect trends in CFC and FFC (2015 to 2022), marking land cover transitions in significant LPD areas. These calculations were performed using Python libraries "pymannkendall" and "rasterio". To analyze potential LCC change characteristics across the boundary at "Boundary", we separately computed the distributions of slope for the entire GGW region, south of "Boundary", and north of "Boundary", considering significant M-K trends. Given the apparent skewness in the distributions of slope, we employed the M-W test to examine the differences under various conditions. Then use Cliff's Delta to evaluate the degree of difference. Finally, by analyzing the inflow and outflow patterns of cropland and forestland in areas with significant changes in land productivity (LPD increase and decrease classes), and calculating the proportions of LP increase and decrease for each type of conversion, we identified how these transitions influence trends in land productivity change.

Data availability

The datasets analyzed in this study are publicly available. The ERA5-Land Daily Aggregated dataset is available as the GEE Collection Snippet: ECMWF/ERA5_LAND/DAILY_AGGR. To assess the driving effect of land use type change on LPD, Google's DYNAMIC WORLD V1 dataset is available as the GEE Collection Snippet: GOOGLE/DYNAMICWORLD/V1. We use the CO2 dataset released by Zenodo (downloaded from https://zenodo.org/records/5021361 60). We select data from 2015 to 2022 based on the SSP-126 assumptions. We choose the NDE dataset generated by NASA Goddard Institute for Space Studies (GISS) in the Atmospheric Chemistry and Climate Model Intercomparison Project (ACCMIP) based on RCP60 (downloaded from https://data.ceda.ac.uk/badc/accmip/data/GISS/GISS-E2-R/accrcp60/ACCMIP-monthly/r1i1p3/v1). The Aridity index (AI) data can be obtained from the FAO website [https://data.apps.fao.org/catalog/dataset/221072ae-2090-48a1-be6f-5a8

8f061431a/resource/7563c7fa-03aa-4141-92ef-8aa4236fb9a4] (https://data.apps.fao.org/catalog/dataset/221072ae-2090-48a1-be6f-5a88f061431a/resource/7563c7fa-03aa-4141-92ef-8aa4236fb9a4).

Received: 20 March 2025; Accepted: 4 September 2025

Published online: 07 October 2025

References

- 1. Economics of Land Degradation and Improvement A Global Assessment for Sustainable Development (Springer International Publishing, 2016). https://doi.org/10.1007/978-3-319-19168-3.
- 2. The Great Green. Wall Implementation Status and Way ahead To 2030 (UNCCD, 2020).
- 3. Yang, Z., Gao, X., Lei, J., Meng, X. & Zhou, N. Analysis of Spatiotemporal changes and driving factors of desertification in the Africa Sahel. *CATENA* 213, 106213 (2022).
- 4. Epule, T. E., Ford, J. D., Lwasa, S. & Lepage, L. Climate change adaptation in the Sahel. Environ. Sci. Policy. 75, 121-137 (2017).
- Ogutu, B. O., D'Adamo, F. & Dash, J. Impact of vegetation greening on carbon and water cycle in the African Sahel-Sudano-Guinean region. Glob. Planet Change. 202, 103524 (2021).
- Souverijns, N. et al. Thirty years of land cover and fraction cover changes over the Sudano-Sahel using landsat time series. Remote Sens. https://doi.org/10.3390/rs12223817 (2020).
- 7. Mirzabaev, A., Sacande, M., Motlagh, F., Shyrokaya, A. & Martucci, A. Economic efficiency and targeting of the African great green wall. *Nat. Sustain.* 5, 17–25 (2021).
- 8. FAO. The Future of Food and Agriculture: Trends and Challenges (Food and Agriculture Organization of the United Nations, 2017).
- 9. Goffner, D., Sinare, H. & Gordon, L. J. The great green wall for the Sahara and the Sahel initiative as an opportunity to enhance resilience in Sahelian landscapes and livelihoods. *Reg. Environ. Change.* 19, 1417–1428 (2019).
- Prince, S. D. Challenges for remote sensing of the sustainable development goal SDG 15.3.1 productivity indicator. Remote Sens. Environ. 234, 111428 (2019).
- Global sustainable development report briefs. (2015). https://sustainabledevelopment.un.org/content/documents/1870GSDR%20 2015%20Briefs.pdf
- Gadzama, N. M. Attenuation of the effects of desertification through sustainable development of great green wall in the Sahel of Africa. WISTSD 14, 279–289 (2017).
- 13. Get Africa's. Great green wall back on track. Nature 587, 8-8 (2020).
- 14. How to make Africa's 'Great Green Wall' a success. Nature 605, 8-8 (2022).
- 15. Sims, N. et al. Version 2.0 Citation. https://www.unccd.int/sites/default/files/documents/2021-09/UNCCD_GPG_SDG-Indicator-15.3.1_version2_2021.pdf
- 16. Sachs, J., Kroll, C., Lafortune, G., Fuller, G. & Woelm, F. Sustainable Development Report 2022 (Cambridge University Press, 2022). https://doi.org/10.1017/9781009210058
- 17. Leroux, L., Bégué, A., Lo Seen, D., Jolivot, A. & Kayitakire, F. Driving forces of recent vegetation changes in the sahel: lessons learned from regional and local level analyses. *Remote Sens. Environ.* **191**, 38–54 (2017).
- 18. Sedano, F., Molini, V. & Azad, M. A. K. A mapping framework to characterize land use in the Sudan-Sahel region from dense stacks of landsat data. *Remote Sens.* 11, 648 (2019).
- 19. Huang, K. et al. Enhanced peak growth of global vegetation and its key mechanisms. Nat. Ecol. Evol. 2, 1897-1905 (2018).
- 20. Zhu, Z. et al. Greening of the Earth and its drivers. Nat. Clim. Change. 6, 791-795 (2016).
- 21. Almalki, R., Khaki, M., Saco, P. M. & Rodriguez, J. F. Monitoring and mapping vegetation cover changes in arid and Semi-Arid areas using remote sensing technology: A review. *Remote Sens.* 14, 5143 (2022).
- 22. Martiny, N., Camberlin, P., Richard, Y. & Philippon, N. Compared regimes of NDVI and rainfall in semi-arid regions of Africa. *Int. J. Remote Sens.* 27, 5201–5223 (2006).
- 23. Shen, T. et al. HiLPD-GEE: high Spatial resolution land productivity dynamics calculation tool using Landsat and MODIS data. *Int. J. Digit. Earth.* 16, 671–690 (2023).
- 24. Overview of Land Degradation Neutrality (LDN) in Europe and Central Asia. (FAO. (2022). https://doi.org/10.4060/cb7986en
- 25. Ivits, E. et al. European Commission Joint research centre. In Land-Productivity Dynamics Towards Integrated Assessment of Land Degradation at Global Scales (Publications Office, 2013).
- 26. Michael, C. et al. World Atlas of Desertification. (2018). https://doi.org/10.2760/06292
- 27. Grömping, U. Relative importance for linear regression in R: the package relaimpo. J Stat. Soft 17, 1-27 (2006).
- 28. Rotllan-Puig, X., Ivits, E. & Cherlet, M. LPDynR: A new tool to calculate the land productivity dynamics indicator. *Ecol. Ind.* 133, 108386 (2021).
- 29. Jian, D. et al. Limited driving of elevated CO₂ on vegetation greening over global drylands. *Environ. Res. Lett.* **18**, 104024 (2023).
- 30. Yang, Y. et al. Factors affecting Long-Term trends in global NDVI. Forests 10, 372 (2019).
- 31. Chen, T. et al. The greening and wetting of the Sahel have leveled off since about 1999 in relation to SST. Remote Sens. 12, 2723 (2020).
- 32. Brandt, M. et al. Assessing Woody vegetation trends in Sahelian drylands using MODIS based seasonal metrics. *Remote Sens. Environ.* 183, 215–225 (2016).
- 33. Wu, S., Gao, X., Lei, J., Zhou, N. & Wang, Y. Spatial and Temporal changes in the normalized difference vegetation index and their driving factors in the desert/grassland biome transition zone of the Sahel region of Africa. *Remote Sens.* 12, 4119 (2020).
- 34. Jiang, M., Jia, L., Menenti, M. & Zeng, Y. Understanding Spatial patterns in the drivers of greenness trends in the Sahel-Sudano-Guinean region. *Big Earth Data*. 7, 298–317 (2023).
- 35. Zeng, Y. et al. Regional divergent evolution of vegetation greenness and Climatic drivers in the Sahel-Sudan-Guinea region: nonlinearity and explainable machine learning. Front. Glob Change. 7, 1416373 (2024).
- 36. Adenle, A. A., Eckert, S., Adedeji, O. I., Ellison, D. & Speranza, C. I. Human-induced land degradation dominance in the Nigerian Guinea Savannah between 2003–2018. Remote Sens. Applications: Soc. Environ. 19, 100360 (2020).
- 37. Nyamekye, C. et al. Usage of MODIS NDVI to evaluate the effect of soil and water conservation measures on vegetation in Burkina Faso. *Land. Degrad. Dev.* 32, 7–19 (2021).
- 38. Guo, W. Q., Yang, T. B., Daí, J. G., Shi, L. & Lu, Z. Y. Vegetation cover changes and their relationship to climate variation in the source region of the yellow river, china, 1990–2000. *Int. J. Remote Sens.* 29, 2085–2103 (2008).
- 39. Piao, S. et al. Characteristics, drivers and feedbacks of global greening. Nat. Rev. Earth Environ. 1, 14-27 (2019).
- Zhang, Y. et al. Increasing sensitivity of dryland vegetation greenness to precipitation due to rising atmospheric CO2. Nat. Commun. 13, 4875 (2022).
- 41. Seddon, A. W. R., Macias-Fauria, M., Long, P. R., Benz, D. & Willis, K. J. Sensitivity of global terrestrial ecosystems to climate variability. *Nature* 531, 229–232 (2016).
- 42. Nemani, R. R. et al. Climate-Driven increases in global terrestrial net primary production from 1982 to 1999. Sci. New. Ser. 300, 1560–1563 (2003).
- 43. Brandt, M. et al. Changes in rainfall distribution promote Woody foliage production in the Sahel. Commun. Biol. 2, 133 (2019).

- 44. Soumare, S., Andrieu, J., Fall, A., Diaw, E. H. B. & Descroix, L. Spatial and Temporal analysis of Rain-NDVI relationship in lower and middle Casamance from 1982 to 2019. *Remote Sens. Earth Syst. Sci.* 5, 246–262 (2022).
- Cho, J., Lee, Y. & Lee, H. The effect of precipitation and air temperature on land-cover change in the Sahel. Water Environ. J. 29, 439–445 (2015).
- 46. Greaver, T. L. et al. Key ecological responses to nitrogen are altered by climate change. Nat. Clim. Change. 6, 836-843 (2016).
- 47. Burrell, A. L., Evans, J. P. & De Kauwe, M. G. Anthropogenic climate change has driven over 5 million km2 of drylands towards desertification. *Nat. Commun.* 11, 3853 (2020).
- 48. Olorunfemi, I. E., Olufayo, A. A., Fasinmirin, J. T. & Komolafe, A. A. Dynamics of land use land cover and its impact on carbon stocks in Sub-Saharan africa: an overview. *Environ. Dev. Sustain.* 24, 40–76 (2022).
- 49. Herrmann, S. M., Brandt, M., Rasmussen, K. & Fensholt, R. Accelerating land cover change in West Africa over four decades as population pressure increased. *Commun. Earth Environ.* 1, 53 (2020).
- 50. Wood, E. C., Tappan, G. G. & Hadj, A. Understanding the drivers of agricultural land use change in south-central Senegal. *J. Arid Environ.* 59, 565–582 (2004).
- 51. Osman, A. K. & Ali, A. M. Sudan Land, climate, energy, agriculture and development: A study in the Sudano-Sahel initiative for regional development, jobs, and food security. SSRN J. https://doi.org/10.2139/ssrn.3769148 (2021).
- 52. Sulieman, H. M. Agricultural land use change and its drivers in the Sudanese Ethiopian borderland: the case of Al-Fashaga region. *Geol. Ecol. Landscapes.* 1–11. https://doi.org/10.1080/24749508.2024.2430038 (2024).
- 53. Curtis, P. G., Slay, C. M., Harris, N. L., Tyukavina, A. & Hansen, M. C. Classifying drivers of global forest loss. Science 361, 1108–1111 (2018).
- Nzabarinda, V. et al. Impact of cropland development intensity and expansion on natural vegetation in different African countries. *Ecol. Inf.* 64, 101359 (2021).
- 55. Jayne, T. S. & Sanchez, P. A. Agricultural productivity must improve in sub-Saharan Africa. Science 372, 1045–1047 (2021).
- 56. Trichon, V., Hiernaux, P., Walcker, R. & Mougin, E. The persistent decline of patterned Woody vegetation: the tiger Bush in the context of the regional Sahel greening trend. *Glob. Change Biol.* 24, 2633–2648 (2018).
- 57. Brown, C. F. et al. Dynamic world, near real-time global 10 m land use land cover mapping. Sci. Data. 9, 251 (2022).
- 58. Cheng, W. et al. Global monthly gridded atmospheric carbon dioxide concentrations under the historical and future scenarios. *Sci. Data.* **9**, 83 (2022).
- 59. Middleton, N. & Thomas, D. World atlas of desertification. (1993).
- 60. Didan, K., Munoz, A. B. & Huete, A. MODIS Vegetation Index User's Guide (MOD13 Series).
- 61. Cliff, N. Dominance Statistics: Ordinal Analyses to Answer Ordinal Questions.
- 62. Vispoel, W. P. & Shavelson, R. J. Statistical reasoning for the behavioral sciences. J. Educational Stat. 15, 179 (1990).
- 63. Cohen, J. The Earth is round (p < . 05): rejoinder. Am. Psychol. 50, 1103-1103 (1995).
- 64. Mangiafico, S. S. Summary and analysis of extension program evaluation in r.

Acknowledgements

The findings and conclusions in this publication are those of the authors and should not be construed to represent any official USDA or U.S. Government determination or policy.

Author contributions

X.L. conceived and designed the experiments. Y.Z., T.S., Q.L., and A.T.K.-B. analyzed the data and performed the experiments. Y.Z., X.L., G.M., A.G., and Y.P. wrote the main manuscript. All authors reviewed the manuscript.

Declarations

Competing interests

The authors declare no competing interests.

Additional information

Supplementary Information The online version contains supplementary material available at https://doi.org/1 0.1038/s41598-025-18963-2.

Correspondence and requests for materials should be addressed to X.L. or Y.P.

Reprints and permissions information is available at www.nature.com/reprints.

Publisher's note Springer Nature remains neutral with regard to jurisdictional claims in published maps and institutional affiliations.

Open Access This article is licensed under a Creative Commons Attribution-NonCommercial-NoDerivatives 4.0 International License, which permits any non-commercial use, sharing, distribution and reproduction in any medium or format, as long as you give appropriate credit to the original author(s) and the source, provide a link to the Creative Commons licence, and indicate if you modified the licensed material. You do not have permission under this licence to share adapted material derived from this article or parts of it. The images or other third party material in this article are included in the article's Creative Commons licence, unless indicated otherwise in a credit line to the material. If material is not included in the article's Creative Commons licence and your intended use is not permitted by statutory regulation or exceeds the permitted use, you will need to obtain permission directly from the copyright holder. To view a copy of this licence, visit https://creativecommons.org/licenses/by-nc-nd/4.0/.

© The Author(s) 2025